NANO LETTERS

pubs.acs.org/NanoLett Letter

Epitaxial Electrodeposition of Fe with Controlled In-Plane Variants for a Reversible Metal Anode in an Aqueous Electrolyte

Chenxi Sui, Ching-Tai Fu, Guangxia Feng, Yuqi Li, Junyan Li, Gangbin Yan, Po-Chun Hsu, Steven Chu, and Yi Cui*

Cite This: *Nano Lett.* 2026, 26, 801−808 Read Online

ABSTRACT: The development of reversible metal anodes is a key challenge for advancing aqueous battery technologies, particularly for scalable and safe stationary energy storage applications. Here we demonstrate a strategy to realize epitaxial electrodeposition of iron (Fe) on single-crystal copper (Cu) substrates in aqueous electrolytes. We compare the electrodeposition behavior of Fe on polycrystalline and single-crystalline Cu substrates, revealing that the latter enables highly uniform, dense, and crystallographically aligned Fe growth. Comprehensive electron backscatter diffraction and X-ray diffraction analyses confirm the formation of Fe with specific out-of-plane and in-plane orientations, including well-defined rotational variants. Our findings highlight that epitaxial electrodeposition of Fe can suppress dendritic growth and significantly enhance the Coulombic efficiency during plating/stripping cycles. This approach bridges fundamental crystallography with practical electrochemical performance, providing a pathway toward high-efficiency aqueous batteries utilizing Earth-abundant materials.

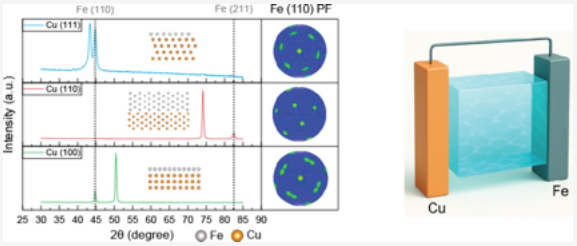

KEYWORDS: *epitaxy, aqueous battery, crystallography, epitaxial electrodeposition*

Aqueous batteries are gaining attention for scalable stationary energy storage due to their intrinsic safety, low cost, and environmental compatibility.[1−7] Among various chemistries, iron-based aqueous batteries are especially attractive given the abundance and affordability of iron,[8] along with the well-established infrastructure of the steel industry that enables scalable implementation. Despite these advantages, iron metal anodes face critical challenges in achieving reversible electrochemical cycling.[8−13] Issues such as dendritic growth, hydrogen evolution, and a low Coulombic efficiency (CE) hinder their technical advancement. Improving the morphology and reversibility of iron plating and stripping is essential for enabling high-performance aqueous iron batteries.

Epitaxial electrodeposition offers a potential solution by promoting crystallographically aligned growth of metal layers.[8,13−23] By matching the deposited metal's orientation with that of the substrate, epitaxy can reduce nucleation barriers, suppress dendrites, and enable more uniform deposition. Electrochemical epitaxy differs fundamentally from traditional vapor-phase epitaxy in both mechanism and implications. In vapor-phase epitaxy, atoms arrive on the substrate in a high-energy, uncoordinated state and require high-temperature annealing to diffuse into thermodynamically favorable lattice positions. This process is typically irreversible and sensitive to kinetic trapping. In contrast, electrochemical epitaxy proceeds through solvated redox-active species (e.g., Fe^{2+}) in the electrolyte. Prior to metal incorporation, such cations must approach the electrified interface, undergo partial desolvation, and/or form specifically adsorbed intermediates within the inner Helmholtz layer, where adsorption is known to occur on well-defined crystallographic sites on single-crystal electrodes (e.g., commensurate overlayers and underpotential deposition on low-index surfaces).[24] In this framework, the substrate lattice and surface symmetry can template the earliest nucleation events and lower the effective nucleation barrier for registered nuclei on commensurate sites, thereby promoting oriented growth. While the detailed solvation−desolvation and electron-transfer pathway is complex and electrolyte-dependent, recent theoretical and atomistic perspectives emphasize that the interfacial solvation structure and ion desolvation dynamics can strongly influence electrochemical growth and surface-adsorbed nanostructures.[25] Moreover, the electrochemical process is inherently reversible, allowing the controlled cycling of Fe deposition and dissolution (Table 1).

In this work, we demonstrate that aqueous electrodeposition of Fe on single-crystalline Cu substrates can result in epitaxial

Received: October 21, 2025
Revised: January 4, 2026
Accepted: January 6, 2026
Published: January 9, 2026

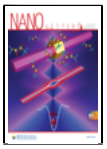

https://doi.org/10.1021/acs.nanolett.5c05270
Nano Lett. 2026, 26, 801−808

Table 1. Comparison between Traditional Vapor-Phase Epitaxy and Electrochemical Epitaxy

Epitaxy type	Traditional (vapor phase) epitaxy	Electrochemical epitaxy
Representation Fe Transition state Fe Undiffused Fe	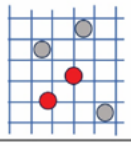	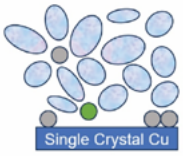
Epitaxy mechanism	Need annealing to allow Fe diffuse to thermodynamically favorable sites	Fe^{2+} surrounded by hydration shells, may have already diffused to the corresponding sites
Redox chemical reaction	no	yes, Fe^{2+} to Fe
Hydration shell	no	yes
Reversibility	Not reversible	reversible

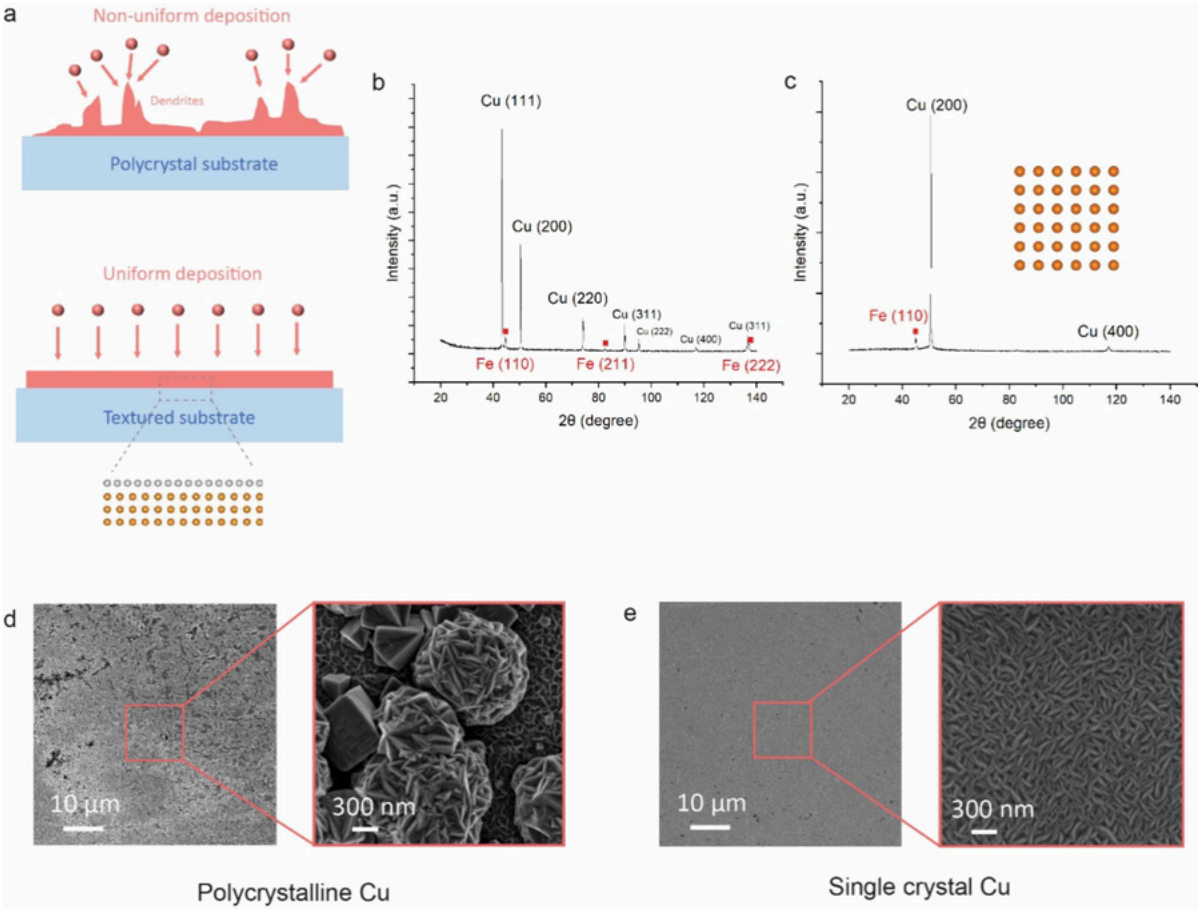

Figure 1. Electrodeposition of Fe on polycrystalline and single-crystal Cu substrates. (a) Schematic illustration comparing the metal deposition morphology on polycrystalline versus textured (e.g., single-crystalline) Cu substrates. (b and c) XRD 2θ scans of Fe electrodeposited on polycrystalline Cu and single-crystal Cu (100), respectively. The inset in part c shows the atomic arrangement of the Cu (100) surface. (d and e) SEM images of Fe films deposited on polycrystalline and single-crystal Cu substrates, respectively, highlighting the improved uniformity and compactness achieved with epitaxial growth.

https://doi.org/10.1021/acs.nanolett.5c05270
Nano Lett. 2026, 26, 801−808

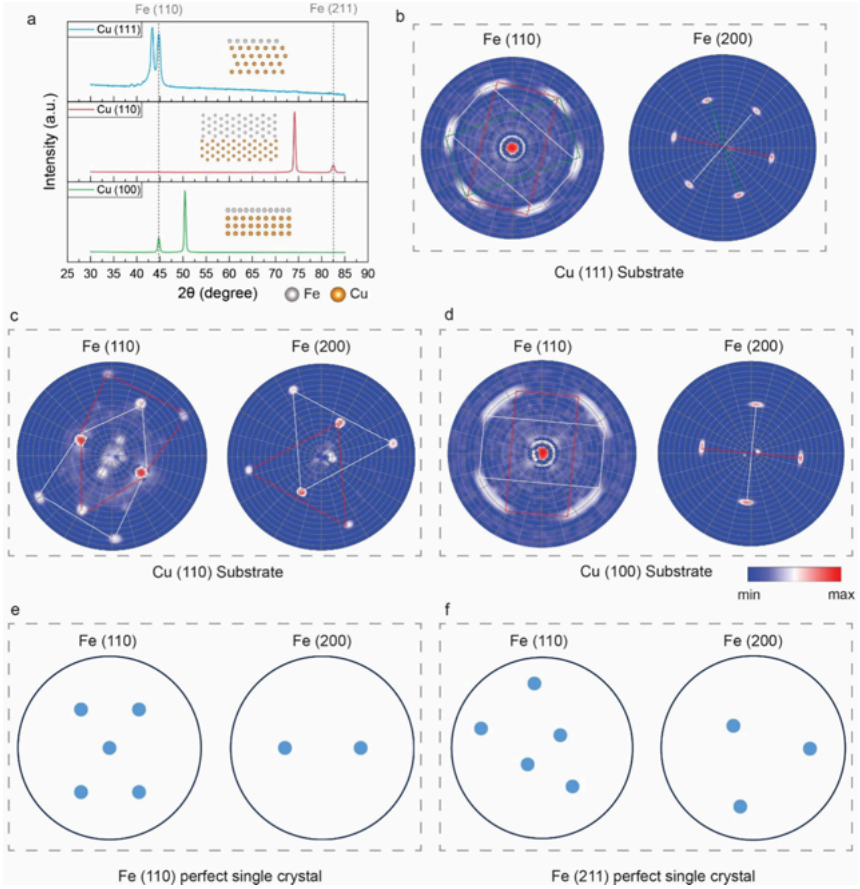

Figure 2. Crystallographic characterization of electrodeposited Fe on different single-crystal Cu substrates. (a) XRD 2θ scans of Fe films electrodeposited on Cu (111), Cu (100), and Cu (110), showing the preferred out-of-plane orientations. The three insets adjacent to the diffraction patterns illustrate the atomic arrangements of Fe (110) on Cu (111), Fe (211) on Cu (110), and Fe (110) on Cu (100), respectively. (b–d) Experimental XRD pole figures of Fe deposited on Cu (111), Cu (110), and Cu (100), respectively. Each sample includes two pole figures corresponding to the 2θ Fe (110) and Fe (200) 2θ angles. Colored lines are used to highlight individual sets of epitaxial orientations; each color denotes one distinct rotational variant of single-crystal Fe. (e and f) Simulated pole figures of ideal single-crystal Fe with (110) and (211) orientations, used as references for identifying twinning and in-plane variants in the experimental data.

growth with a well-defined crystallographic orientation and in-plane alignment. Through comprehensive structural characterization, we reveal the existence of specific orientation relationships and twinning phenomena. Electrochemical tests show that such epitaxial control enhances plating–stripping reversibility and suppresses dendrite formation. Our study presents a platform for integrating crystallographic control into aqueous battery design, bridging the gap between materials science and practical energy storage technology.

Variations in the atomic arrangement and crystallographic orientation across substrates significantly influence the morphology and crystallinity of electrodeposited metals. On polycrystalline substrates, where grain orientations are randomly distributed and surface atomic configurations are heterogeneous, metal nucleation tends to occur stochastically. This often results in irregular growth, poor crystallinity, and the formation of dendritic structures. Dendrites increase the electrode's surface area, which enhances undesired side reactions such as hydrogen evolution. Additionally, dendritic deposits can mechanically destabilize the electrode by penetrating the separator or detaching during stripping, thereby reducing the electrochemical reversibility of the system.

In contrast, when the substrate is engineered to be textured or single-crystalline, with a uniform lattice orientation and well-ordered surface atoms, electrodeposition proceeds in a more controlled and uniform manner. Under such conditions, the deposited metal can adopt a preferential orientation, and in favorable cases, epitaxial growth is achieved (Figure 1a). This structural coherence at the interface contributes to a smoother morphology, reduced dendrite formation, and improved cycling stability.

To highlight this effect, we performed electrodeposition of Fe on both polycrystalline Cu and single-crystal Cu (100) substrates. The X-ray diffraction (XRD) 2θ scan of Fe deposited on polycrystalline Cu (Figure 1b) reveals multiple diffraction peaks—Fe (110), Fe (211), and Fe (222)—indicative of randomly oriented grains. This structural disorder is reflected in the rough and inhomogeneous surface morphology observed in the scanning electron microscopy (SEM) images (Figure 1d). In contrast, Fe electrodeposited on Cu (100) displays a single Fe (110) diffraction peak (Figure

https://doi.org/10.1021/acs.nanolett.5c05270
Nano Lett. 2026, 26, 801–808

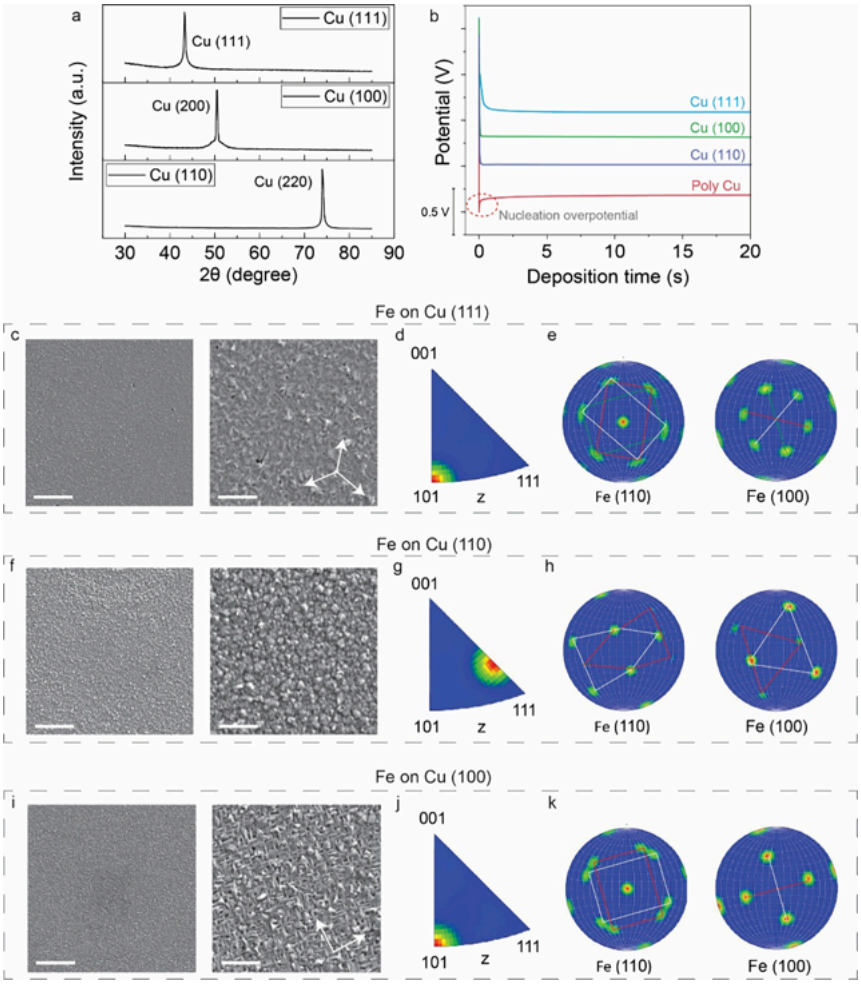

Figure 3. Characterization of Fe electrodeposition. (a) XRD 2θ scan of single-crystal Cu. (b) Voltage−time curves of Fe electrodeposition under a constant current, 10 mA cm^{-2}. (c, f, and i) SEM photographs of electrodeposited Fe on single-crystal Cu (111), Cu (110), and Cu (100). The scale bars in the photographs on the right are 5 μm and 500 nm. (d, g, and j) EBSD inverse pole figures and (e, h, and k) EBSD pole figures of electrodeposited Fe on single-crystal Cu (111), Cu (110), and Cu (100).

1c), consistent with a highly oriented film. The corresponding SEM image (Figure 1e) shows a dense and uniform morphology characteristic of coherent growth guided by the underlying substrate.

Inspired by the morphology uniformity improvement of using single-crystal Cu as the substrate, we went further to study the Fe electrodeposition on single-crystal Cu substrates with three different orientations of (100), (110), and (111), respectively. To evaluate the crystallographic quality of electrodeposited Fe films on a larger spatial scale, XRD was employed. Compared to electron backscatter diffraction (EBSD), which typically probes micrometer-scale regions, the XRD beam spot size (~6 mm) enables more global structural characterization. Figure 2a presents the 2θ scans of Fe films deposited on single-crystal Cu substrates with different orientations. For both Cu (111) and Cu (100) substrates, the Fe films exhibit a dominant (110) out-of-plane orientation, indicating a preferential crystallographic alignment. In contrast, Fe electrodeposited on Cu (110) shows a dominant Fe (211) peak, suggesting that the substrate orientation plays a critical role in guiding the film texture. To illustrate ideal epitaxial single-crystal growth, atomic schematics of Fe epitaxy on Cu are shown next to each diffraction pattern. To further assess the full crystallographic orientation, particularly the in-plane alignment, we performed XRD pole figure measurements for all three substrate types. These were compared with simulated pole figures of ideal single-crystalline Fe (110) and Fe (211) (Figure 2e,f) to identify the degree of twinning and the presence of rotational variants. On Cu (111), the Fe (110) pole figure (Figure 2b) reveals three sets of well-defined poles arranged with 120° in-plane rotation, consistent with the 3-fold symmetry and the formation of three rotational variants. On Cu (100), Fe (110) is again the preferred orientation, but the pole figure (Figure 2d) shows two rotational variants separated by 90°, reflecting the underlying 2-fold symmetry of the Fe. Remarkably, electrodeposition on Cu (110) yields Fe films with a high-index (211) orientation. The corresponding pole figure (Figure 2c) exhibits two sets of Fe (211) poles with 180° rotational symmetry, indicating the presence of twin domains with a well-defined orientation. Although the Fe

https://doi.org/10.1021/acs.nanolett.5c05270
Nano Lett. 2026, 26, 801−808

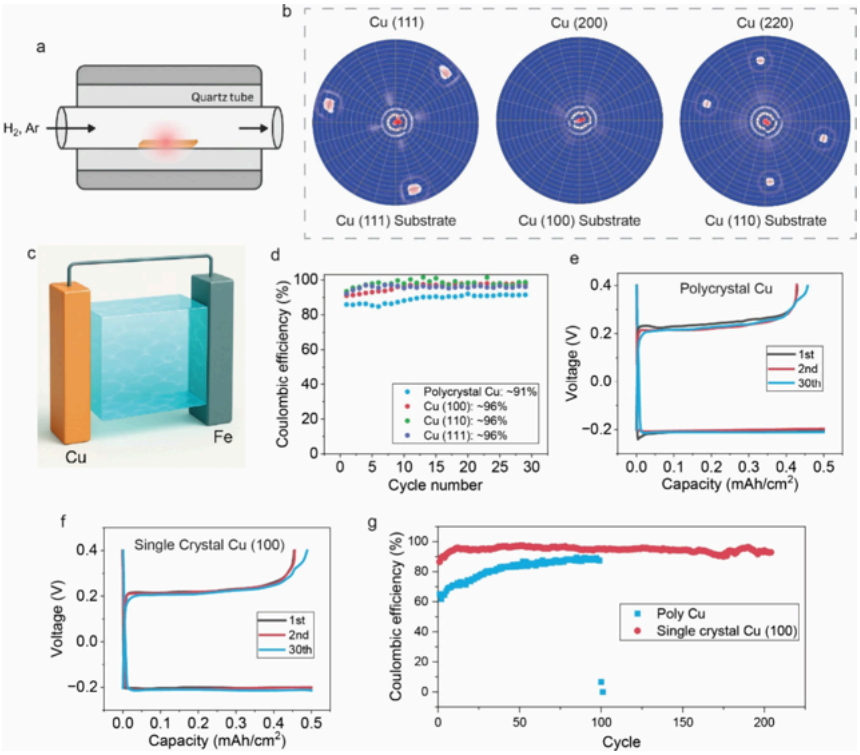

Figure 4. Electrochemical reversibility of Fe||Cu asymmetric coin cells using different Cu substrates. (a) Schematic illustration of the annealing process used to convert polycrystalline Cu into textured Cu. (b) XRD pole figures of annealed Cu foil, indicating the formation of a highly textured (though not perfect single-crystal) surface. (c) Schematic of the Fe||Cu coin cell configuration used for reversibility testing. (d) CE comparison of Fe||Cu cells assembled with polycrystalline Cu and single-crystal Cu (100) electrodes, cycled at 0.5 mA cm^{-2}. The cutoff voltage is set at 0.4 V. (e and f) Representative charge−discharge voltage profiles for cells with polycrystalline Cu and single-crystal Cu (100) electrodes, respectively. (g) Long-term CE stability for Fe||Cu cells showing superior performance and cycling durability with the single-crystal Cu (100) electrode. The cutoff voltage is set at 0.5 V.

deposits on the three Cu substrates are not perfect single crystals, they exhibit well-defined twinning and in-plane rotational variants, reflecting a high degree of crystallographic order and predictable epitaxial behavior.

These observations underscore the capacity of electrochemical epitaxy to produce highly regulated crystallographically aligned Fe films, including those with high-index orientations that are typically difficult to synthesize. The presence of controlled twinning and discrete in-plane variants further highlights the epitaxial nature of the growth, even in a body-centered-cubic system, where such order is rarely observed under ambient conditions. We also did an atomic analysis to provide a theoretical rationale for epitaxial Fe electrodeposition on Cu (Supplementary Discussion 1).

Figure 3a confirms the strong out-of-plane crystallographic alignment of the single-crystal Cu substrate. Electrochemical measurements (Figure 3b) reveal that Fe deposited on polycrystalline Cu exhibits a significantly higher overpotential compared to that of Fe deposited on single-crystal Cu substrates, indicating that a well-textured substrate facilitates more favorable Fe nucleation and growth. This galvanostatic curve was collected at 10 mA cm^{-2} to highlight the overpotential more clearly, whereas all epitaxial electrodeposition samples used for structural characterization were prepared at 1 mA cm^{-2}. SEM images (Figure 3c,f,i) show that Fe electrodeposited on all single-crystal Cu orientations forms dense, uniform, and well-regulated morphologies. Crystallographic orientation mapping using EBSD inverse pole figures (Figure 3d,g,j) indicates that Fe deposited on Cu (111) and Cu (100) adopts a dominant (110) out-of-plane orientation, while deposition on Cu (110) results in a (211) orientation. To assess in-plane orientation, EBSD pole figures were generated (Figure 3e,h,k), showing excellent agreement with the corresponding XRD pole figures in Figure 2. Notably, the EBSD pole figures exhibit higher clarity, likely due to the smaller probe size of EBSD, which minimizes the averaging over defects and misorientations compared to XRD. The symmetry of the in-plane patterns also reflects the morphology growth direction. Fe grown on Cu (111) exhibits 3-fold symmetry, consistent with three equivalent in-plane growth directions separated by 120°, as observed in Figure 3c. On Cu (100), Fe grows along two orthogonal directions separated by 90°, corresponding to the substrate's 2-fold symmetry (Figure 3i). Inverse pole figures and pole figures for all Fe orientations are shown in Figure S1. These growth directions are highlighted with arrows in the respective SEM images. This integrated structural and morphological analysis reveals a strong correlation between the substrate crystallographic orientation and the resulting Fe deposition morphology.

Following the demonstration of high-quality Fe electrodeposition on single-crystal Cu substrates, we explored a more cost-effective approach to obtain crystallographically aligned

https://doi.org/10.1021/acs.nanolett.5c05270
Nano Lett. 2026, 26, 801−808

Cu by annealing commercial polycrystalline Cu foils (Figure 4a). The annealing method follows our previous work.[17] Although the annealed Cu is not a perfect single crystal—as evidenced by the presence of satellite intensities around the main poles in the XRD pole figure (Figure 4b), which indicates the existence of crystallographic defects and minor misorientations—it still exhibits significant texturing. This suggests that while full single crystallinity is not achieved, the substrate retains sufficient orientational coherence to influence subsequent Fe deposition. From a practical perspective, perfect single crystallinity is not a prerequisite for high-performance battery electrodes. Given the trade-off between the fabrication cost and electrochemical performance, a well-textured Cu substrate is often sufficient to achieve substantially improved reversibility in metal plating/stripping processes.

To assess the electrochemical impact of substrate crystallinity, we assembled Fe||Cu asymmetric coin cells using both polycrystalline and annealed single-crystal Cu electrodes (Figure 4c). Galvanostatic cycling at a current density of 0.5 mA cm^{-2} in Figure 4d reveals that the annealed single-crystal Cu electrode delivers a higher CE (~96%) compared with its polycrystalline counterpart (~91%). Detailed charge−discharge profiles (Figure 4e,f) show that the polycrystalline Cu exhibits a larger overpotential during stripping, while the single-crystal Cu electrode maintains a more stable voltage behavior, consistent with more uniform Fe deposition and dissolution. Finally, long-term cycling was performed using a Cu (100) single-crystal substrate to evaluate durability (Figure 4g). The coin cell assembled with a polycrystalline Cu electrode short-circuited after approximately 100 cycles due to nonuniform deposition and dendrite-induced failure. In contrast, the cell with the Cu (100) single-crystal electrode maintained a stable performance for over 200 cycles, with no observable degradation and consistently high CE around 96%. Top-view and 45°-tilted (quasi-cross-sectional) SEM before cycling and after 20 cycles shows that Fe deposits on single-crystal Cu (111) remain comparatively flat, dense, and uniform (with only modest coarsening), whereas Fe on polycrystalline Cu is irregular and highly nonuniform both before and after cycling, corroborating improved interfacial stability and reversibility enabled by crystallographic control (Figures S3 and S4).

Additional high-current density/high-loading tests show that 10 mA cm^{-2} significantly weakens Fe epitaxial texture [Fe (211) nearly vanishes in 2θ and the Fe (200) pole-figure intensity drops with defect features], whereas longer deposition at higher areal capacity retains clear epitaxial signatures, and single-crystal Cu still delivers markedly higher CE and longer cycle life than polycrystalline Cu (~80% for 20 cycles vs ~60% for 14 cycles at high current density; ~90% for 50 cycles vs <80% for 34 cycles at high loading; Figure S5). We also performed linear-sweep voltammetry measurements on Fe deposited on different Cu substrates, showing that epitaxial Fe grown on single-crystal Cu exhibits reduced hydrogen evolution reaction (HER) activity compared with Fe on polycrystalline Cu, which likely contributes to the improved cycling stability (Figure S6).

This work demonstrates that epitaxial electrodeposition of Fe on single-crystal and textured Cu substrates provides a promising pathway to achieving structurally uniform, highly reversible metal anodes in aqueous electrochemical systems. Through detailed crystallographic and morphological analyses, we show that single-crystal Cu facilitates the formation of Fe films with well-defined (110) and (211) orientations and in-plane rotational variants, leading to smoother deposition, suppressed dendrite growth, and improved CE compared to those of conventional polycrystalline substrates.

Although this study focused primarily on the materials science aspects—elucidating the growth behavior, orientation control, and structural quality of electrochemically deposited Fe—our findings highlight the broader potential of electrochemical epitaxy in aqueous battery applications. The strategy could be particularly valuable for future anode-free battery designs, where textured metal foils serve as current collectors to guide uniform, reversible metal plating during cycling. In the Supporting Information, we also discuss the substrate requirements for achieving epitaxial electrodeposition and outline potential strategies to suppress HER in future studies (Supplementary Discussion 2 and 3).

Looking forward, a critical challenge lies in scaling up the production of low-cost, large-area, textured metal substrates. While single-crystal Cu offers an ideal platform for fundamental investigation, practical implementation will require accessible methods, such as thermal annealing or directional solidification, to produce industrially viable textured foils. Advancing these capabilities is essential for translating the concept of electrochemical epitaxy into sustainable and scalable technologies for next-generation aqueous batteries.

METHOD

Materials

The single-crystal Cu substrates are purchased from MSE Supplies Inc. $FeSO_4$ and $(NH_4)_2SO_4$ are purchased from Sigma-Aldrich. The aqueous electrolyte is synthesized by mixing 2 M $FeSO_4$ and 0.1 M $(NH_4)_2SO_4$ in deionized water. $(NH_4)_2SO_4$ is used to improve the uniformity of the electrodeposition (Figure S2 and Supplementary Discussion 4). The electrodeposition to grow Fe is done in the water glovebox.

Characterization

The SEM and EBSD characterizations were conducted by a TESCAN LYRA3 field-emission scanning electron microscope with an Oxford Instruments NordlysMax2 electron backscatter diffraction detector at The University of Chicago. The XRD and pole figure were acquired by PANalytical X'Pert 2 in Stanford Nano Shared Facilities. The theoretical pole figures were calculated by *ReciPro* open-source software (https://github.com/seto77/ReciPro).

Textured Cu Annealing

Single-crystal Cu substrates with (111), (100), and (110) orientations were synthesized via the hydrogen-assisted annealing of commercial Cu foils or disks in a quartz tube furnace. For Cu (111), a 25-μm-thick Cu foil was annealed at 1030 °C for 10 h under a 1:1 H_2/Ar mixture (70 sccm each), followed by natural cooling. Cu (100) was prepared by annealing a 3 cm^2, 1-mm-thick Cu disk at 1070 °C for 10 h under a 1:9 H_2/Ar mixture (100/900 sccm), followed by slow cooling to 900 °C at 1 °C min^{-1} and natural cooling. Cu (110) was synthesized by annealing a similar Cu disk at 1030 °C for 10 h under 30 sccm H_2 and 70 sccm Ar, with vacuum pumping applied throughout the process.

Electrochemistry

The electrodeposition is conducted by a VMP3 potentiostat (BioLogic). The current density used to prepare epitaxy

https://doi.org/10.1021/acs.nanolett.5c05270
Nano Lett. 2026, 26, 801−808

samples is set as 1 mA cm^{-2}. The half-cell performance was tested in a coin cell (CR2032) using glassy fiber as a separator and run by the Land BT2000 battery test system. The cell was cycled at 0.5 mA cm^{-2}.

■ ASSOCIATED CONTENT

Data Availability Statement

All data needed to support the conclusions in the paper are present in the manuscript and/or Supporting Information. Additional data related to this paper may be requested from the corresponding authors.

Supporting Information

The Supporting Information is available free of charge at https://pubs.acs.org/doi/10.1021/acs.nanolett.5c05270.

Detailed EBSD data on epitaxial Fe electrodeposition, additional characterization of cycled electrodes, and supplementary discussions (PDF)

■ AUTHOR INFORMATION

Corresponding Author

Yi Cui − *Department of Materials Science and Engineering and Department of Energy Science and Engineering, Stanford University, Stanford, California 94305, United States; Stanford Institute for Materials and Energy Sciences, SLAC National Accelerator Laboratory, Menlo Park, California 94025, United States;* orcid.org/0000-0002-6103-6352; Email: yicui@stanford.edu

Authors

Chenxi Sui − *Department of Materials Science and Engineering, Stanford University, Stanford, California 94305, United States;* orcid.org/0000-0003-2244-8431

Ching-Tai Fu − *Pritzker School of Molecular Engineering, University of Chicago, Chicago, Illinois 60637, United States*

Guangxia Feng − *Department of Materials Science and Engineering, Stanford University, Stanford, California 94305, United States;* orcid.org/0000-0002-1448-8815

Yuqi Li − *Department of Materials Science and Engineering, Stanford University, Stanford, California 94305, United States;* orcid.org/0000-0003-1501-1549

Junyan Li − *Department of Materials Science and Engineering, Stanford University, Stanford, California 94305, United States*

Gangbin Yan − *Department of Physics, Stanford University, Stanford, California 94305, United States*

Po-Chun Hsu − *Pritzker School of Molecular Engineering, University of Chicago, Chicago, Illinois 60637, United States;* orcid.org/0000-0002-6509-9377

Steven Chu − *Department of Physics and Department of Molecular and Cellular Physiology, Stanford University, Stanford, California 94305, United States; Department of Energy Science and Engineering, Stanford University, Stanford, California 94305, United States*

Complete contact information is available at: https://pubs.acs.org/10.1021/acs.nanolett.5c05270

Author Contributions

Y.C. and C.S. conceived the idea. C.S. performed all of the experiments and the corresponding data analyses. C.-T.F. and C.S. did the EBSD and atomistic modeling. C.S. and Y.C. wrote the manuscript with input from all coauthors.

Notes

The authors declare no competing financial interest.

■ ACKNOWLEDGMENTS

This work is supported by the Aqueous Battery Consortium, an energy innovation hub under the U.S. Department of Energy, Office of Basic Energy Sciences, Division of Materials Science and Engineering. Part of this work was performed at the Stanford Nano Shared Facilities and the Stanford Nanofabrication Facility.

■ REFERENCES

(1) Ahn, H.; Kim, D.; Lee, M.; Nam, K. W. Challenges and possibilities for aqueous battery systems. *Communications Materials* **2023**, *4*, 37.

(2) Chao, D.; et al. Roadmap for advanced aqueous batteries: From design of materials to applications. *Science Advances* **2020**, *6*, No. eaba4098.

(3) Liang, Y.; Yao, Y. Designing modern aqueous batteries. *Nature Reviews Materials* **2023**, *8*, 109−122.

(4) Yan, J.; et al. Rechargeable hybrid aqueous batteries. *J. Power Sources* **2012**, *216*, 222−226.

(5) Zhang, K.; et al. A comprehensive evaluation of battery technologies for high−energy aqueous batteries. *Small* **2024**, *20*, 2309154.

(6) Li, Y.; et al. In situ formation of liquid crystal interphase in electrolytes with soft templating effects for aqueous dual-electrode-free batteries. *Nature Energy* **2024**, *9*, 1350−1359.

(7) Greenburg, L. C.; et al. Crowding agent stabilizes aqueous electrolyte for reversible iron metal anode. *ACS Energy Letters* **2025**, *10*, 1022−1029.

(8) Wu, X.; et al. A rechargeable battery with an iron metal anode. *Adv. Funct. Mater.* **2019**, *29*, 1900911.

(9) Fuller, S. T.; et al. Engineering electrodeposition for next-generation batteries. *Electrochemical Society Interface* **2024**, *33*, 55.

(10) Gong, K.; et al. All-soluble all-iron aqueous redox-flow battery. *ACS Energy Letters* **2016**, *1*, 89−93.

(11) He, Z.; et al. Iron metal anode for aqueous rechargeable batteries. *Materials Today Advances* **2021**, *11*, 100156.

(12) Jiang, J.; Liu, J. Iron anode-based aqueous electrochemical energy storage devices: Recent advances and future perspectives. *Interdisciplinary Materials* **2022**, *1*, 116−139.

(13) Wei, L.; Wu, M. C.; Zhao, T. S.; Zeng, Y. K.; Ren, Y. X. An aqueous alkaline battery consisting of inexpensive all-iron redox chemistries for large-scale energy storage. *Applied Energy* **2018**, *215*, 98−105.

(14) Liu, R.; Oba, F.; Bohannan, E. W.; Ernst, F.; Switzer, J. A. Shape control in epitaxial electrodeposition: Cu2O nanocubes on InP(001). *Chem. Mater.* **2003**, *15*, 4882−4885.

(15) Mahenderkar, N. K.; et al. Epitaxial lift-off of electrodeposited single-crystal gold foils for flexible electronics. *Science* **2017**, *355*, 1203−1206.

(16) Switzer, J. A.; Banik, A. Epitaxial electrodeposition of ordered inorganic materials. *Acc. Chem. Res.* **2023**, *56*, 1710−1719.

(17) Xiao, X.; et al. Epitaxial electrodeposition of zinc on different single crystal copper substrates for high performance aqueous batteries. *Nano Lett.* **2025**, *25*, 1305−1313.

(18) Zheng, J.; et al. Reversible epitaxial electrodeposition of metals in battery anodes. *Science* **2019**, *366*, 645−648.

(19) Sorenson, T. A.; Morton, S. A.; Waddill, G. D.; Switzer, J. A. Epitaxial electrodeposition of Fe3O4 thin films on the low-index planes of gold. *J. Am. Chem. Soc.* **2002**, *124*, 7604−7609.

(20) Kelso, M. V.; Tubbesing, J. Z.; Chen, Q.; Switzer, J. A. Epitaxial electrodeposition of chiral metal surfaces on silicon(643). *J. Am. Chem. Soc.* **2018**, *140*, 15812−15819.

(21) Liu, R.; Vertegel, A. A.; Bohannan, E. W.; Sorenson, T. A.; Switzer, J. A. Epitaxial electrodeposition of zinc oxide nanopillars on single-crystal gold. *Chem. Mater.* **2001**, *13*, 508−512.
(22) Zhang, D.; et al. Ultralow-lattice-mismatched near-zero-strain Zn (0002) anodes for stable zinc metal batteries. *Angew. Chem., Int. Ed.* **2025**, *64*, No. e21269.
(23) Liu, M.; et al. Operando evolution of a hybrid metallic alloy interphase for reversible aqueous zinc batteries. *Angew. Chem., Int. Ed.* **2025**, *64*, No. e202416047.
(24) Schmickler, W.; Santos, E. *Interfacial Electrochemistry*; Springer Science & Business Media, 2010.
(25) Chaudhuri, S.; Maurer, R. J. Challenges in the theory and atomistic simulation of metal electrodeposition. *ACS Electrochemistry* **2025**, *1*, 1014−1032.

https://doi.org/10.1021/acs.nanolett.5c05270
Nano Lett. 2026, 26, 801−808